CENTER FOR CONNECTED AND AUTOMATED TRANSPORTATION

**Project Start Date: Jan 2018**

**Project End Date: April 2019**

**July 2019**

# Driving Etiquette

**by**
**Huei Peng**
**Professor**
**University of Michigan**

UMTRI | The University of Akron | Illinois Center for Transportation | Purdue University | Washtenaw Community College | Central State University

CENTER FOR CONNECTED AND AUTOMATED TRANSPORTATION

DISCLAIMER

Funding for this research was provided by the Center for Connected and Automated Transportation under Grant No. 69A3551747105 of the U.S. Department of Transportation, Office of the Assistant Secretary for Research and Technology (OST-R), University Transportation Centers Program. The contents of this report reflect the views of the authors, who are responsible for the facts and the accuracy of the information presented herein. This document is disseminated under the sponsorship of the Department of Transportation, University Transportation Centers Program, in the interest of information exchange. The U.S. Government assumes no liability for the contents or use thereof.

Suggested APA Format Citation:

Peng, H. & Huang, X. (2019). Driving Etiquette. Final Report. USDOT CCAT Project No. 1
Identifier: http://hdl.handle.net/2027.42/156052

For more information:

Huei Peng
2905 Baxter Road
Ann Arbor, MI 48109
hpeng@umich.edu
(734) 764-6505

**CCAT**
University of Michigan Transportation Research Institute
2901 Baxter Road
Ann Arbor, MI 48109
umtri-ccat@umich.edu
(734) 763-2498

UMTRI | The University of Akron | Illinois Center for Transportation | Purdue University | Washtenaw Community College | Central State University

CENTER FOR CONNECTED AND AUTOMATED TRANSPORTATION

## Technical Report Documentation Page

| 1. Report No. | 2. Government Accession No.<br>Leave blank – not used | 3. Recipient's Catalog No.<br>Leave blank - not used |
|---|---|---|
| **4. Title and Subtitle**<br>Driving Etiquette<br>Identifier:http://hdl.handle.net/2027.42/156052 | | **5. Report Date**<br>July 2019<br>**6. Performing Organization Code**<br>Enter any/all unique numbers assigned to the performing organization, if applicable. |
| **7. Author(s)**<br>Huei Peng, Ph.D. https://orcid.org/0000-0002-7684-1696<br>Xianan Huang. https://orcid.org/0000-0002-1912-4295<br>Final report (Jan 2018-April 2019) | | **8. Performing Organization Report No.**<br>Enter any/all unique alphanumeric report numbers assigned by the performing organization, if applicable. |
| **9. Performing Organization Name and Address**<br>Center for Connected and Automated Transportation<br>University of Michigan Transportation Research Institute<br>2901 Baxter Road<br>Ann Arbor, MI 48109. | | **10. Work Unit No.**<br>**11. Contract or Grant No.**<br>Contract No. 69A3551747105 |
| **12. Sponsoring Agency Name and Address**<br>U.S. Department of Transportation<br>Office of the Assistant Secretary for Research and Technology<br>1200 New Jersey Avenue, SE<br>Washington, DC 20590 | | **13. Type of Report and Period Covered**<br>Final report (Jan 2018-April 2019)<br>**14. Sponsoring Agency Code**<br>OST-R |

**15. Supplementary Notes**
Conducted under the U.S. DOT Office of the Assistant Secretary for Research and Technology's (OST-R) University Transportation Centers (UTC) program.

**16. Abstract**

Establish driving etiquette based on naturalistic driving behavior of human drivers to serve as the basis for the design of autonomous vehicles to drive "like safe human drivers." This project queried a large amount of naturalistic driving data from the Ann Arbor connected vehicle deployment. The data were used to train algorithms to learn about "what is appropriate" based on statistical analysis of human driving behaviors.

| 17. Key Words | 18. Distribution Statement |
|---|---|
| Driver behavior, autonomous vehicles | No restrictions. |

UMTRI · The University of Akron · Illinois Center for Transportation · Purdue University · Washtenaw Community College · Central State University

| 19. Security Classif. (of this report) | 20. Security Classif. (of this page) | 21. No. of Pages | 22. Price |
|---|---|---|---|
| Unclassified | Unclassified | Enter the total number of pages in the report, including both sides of all pages and the front and back covers. | Leave blank – not used |

Form DOT F 1700.7 (8-72) Reproduction of completed page authorized

1. Introduction

Automated vehicles can significantly change the future of ground mobility by reducing crashes, congestion, and fuel consumption. In addition, business model and cost/availability of mobility-on-demand service may also change when automated vehicles become available. Mobility may be more accessible to the elderly and physically challenged population [1]. However, due to the cost differential, it is likely automated vehicles will take a while to reach high market penetration [2]. In the next few decades, these robotic vehicles will operate in an environment interacting with many human-driven vehicles. According to reports from the California Department of Motor Vehicles (DMV) regarding autonomous vehicle on-road testing, most accidents involving automated vehicles are caused by the surrounding human drivers [3]. After examining the crash rate of Waymo and Cruise Automation test fleets released by the California DMV, we hypothesize that these automated vehicles may be partially responsible for these crashes, even when the crashes are largely the responsibility of the other (human-driven) vehicle. The crash report of the Waymo fleet, for example, shows that they were crashed into by other vehicles much more often in 2015-2016 (13), compared with the crash rate of 2017 (3) [4], while the mileage is 636k miles in 2016 and 352k miles in 2017 in California. Assuming the behavior of the surrounding vehicles stay the same, we believe the reduction in crash rate is due to change of behavior of automated vehicle. We hypothesize that it is not only important these vehicles do not crash into other vehicles, it is also important that they "merge into the local driving culture", and do not behave too differently from other (human-driven) vehicles, e.g., inappropriate driving speed, acceleration/deceleration, time headway, gap acceptance during lane-change or left turn, etc. In other words, the robot vehicles must learn the "etiquette" of the local driving culture. In this paper, we report key parameters of human driving behaviors in three scenarios: free-flow driving, car-following, and lane-change/cut-in.

The robotic control of vehicle speed under free flow and car-following scenarios, e.g., applying to Adaptive Cruise Control (ACC), has been studied extensively. Based on the longitudinal dynamics of the vehicle, sliding mode control [6], optimal dynamic back-stepping control [7] and adaptive control [8] have been used to design ACC. Also, car-following range or time headway policy and the influence on traffic were studied for homogeneous platoons [9][10] and mixed traffic [11]. It was found that proper headway policy can guarantee the string stability of platoons. Connected vehicle technologies such as Dedicated Short Range Communications (DSRC) [12] can be used to provide non-line-of-sight information such as platoon leader's acceleration, which enables Cooperative Adaptive Cruise control (CACC) [13]. With the knowledge of the motions of other vehicles, the CACC can stabilize a platoon which was string unstable [14]. However, a substantial portion of the work in the literature do not take human behaviors into consideration [15]. Related advanced driver assistance system (ADAS) work allow the driver to set the desired reference following distance and time headway [16] but the feedback control behavior may not be "human-like".

The lane-change behavior has also been studied extensively. Hatipoglu et al. [17] designed an automated

lane changing controller with a two-layer hierarchical architecture. Ammoun et al. [18] planned the desired lane changing trajectory with speed or acceleration constraints. In [19], Lee et al. proposed an integrated lane-change driver model to control lane changing and lane following maneuvers. In [20], lane-changes on curved roads were studied. In [21], lane-change control under variable speed limits was shown to reduce travel time under various traffic density. However, in the literature whether these controlled lane-change behaviors are compatible with human driving behavior were again largely not studied.

The behavior of human drivers has been collected in large-scale naturalistic field-operational-tests (N-FOTs). Driver characteristics such as time headway, range and range rate were studied [22], [23] and the behaviors were used to identify driver types [24]. Most of the studies in car-following focused on characterizing the control reference point of the human drivers, i.e. the desired car following distance and range rate, or capturing the influence on platoon dynamics [25]. Adaptation of car-following behavior under in-vehicle aid functions is also studied, indicating ADAS can change drivers' behavior significantly [26]. For human lane-change behavior, models usually are based on characteristics such as the range and gap at the initialization of a lane-change [19]. Those models can be used to guide the design of autonomous vehicles. Moreover, in [27][28], the lateral acceleration during lane-changes is captured. The information can guide the design of the lower-level controllers to ensure ride comfort. Finally, in [29], the duration of the lane-change is analyzed. In this paper, we focus on the distribution of the initial range, initial Time to Collision (TTC), the maximum yaw rate of lane-change vehicle, and duration of lane-changes.

Considering both human driver behaviors already analyzed in the literature, as well as information we can extract from the data collected, we defined the key human driver behaviors to be analyzed, which are summarized in TABLE I.

TABLE I KEY BEHAVIOR VARIABLES USEFUL FOR THE DESIGN OF AUTOMATED VEHICLES

| | |
|---|---|
| Control Action Limits | Longitudinal Acceleration<br>Yaw rate During Lane-Changes |
| Free Flow Behavior | Free Flow Speed |
| Car-Following Behavior | Distance to the Lead Vehicle<br>• Mean and Minimum Time Headway<br>• Minimum Time-to-collision (TTC)<br>Dynamic Response to the Lead Vehicle |
| Lane-Change Behavior | Condition to Initialize Lane-Change<br>• Time Headway<br>• Time-to-collision (TTC)<br>Duration of lane-changes |

The main contribution of this work is to learn key control parameters of automated vehicle from human drivers, including: 1)control action limit of automated vehicles for longitudinal control and lane-change; 2)human driver dynamic response and control reference for free flow driving and car-following, which can be used for developing automated vehicle controllers that achieve human-like actions; 3)decision parameter and performance constraint for lane-change. The rest of this paper is organized as follows: Section 2 presents the naturalistic driving database used and the query criteria. Section 3 presents the results for three key scenarios: free-flow, car-following, and lane-changes. Conclusions and future work are given in Section 4.

## 2. Data Description

### 2.1 Naturalistic Driving Database

The data used is from the Safety Pilot Model Deployment (SPMD) project lead by the University of Michigan Transportation Research Institute (UMTRI). SPMD data is collected from 2,800 passenger cars, trucks and buses equipped with DSRC devices to enable Vehicle-to-Vehicle (V2V) and Vehicle-to-Infrastructure (V2I) communications and GPS to track vehicle motions. On the infrastructure side, there were 25 roadside equipment (RSE), 21 at signalized intersections, the remainder at curves and freeway locations. The experiment has been running since August 2012 and has collected more than 5.6 TB of recorded Basic Safety Messages (BSM) including motion (speed, acceleration) and location (longitude, latitude) for all vehicles, Mobileye® and vehicle actuation (brake applied, traction control, etc.) information for some vehicles [30]. A sample of logged BSM locations for one day is shown in Fig. 1

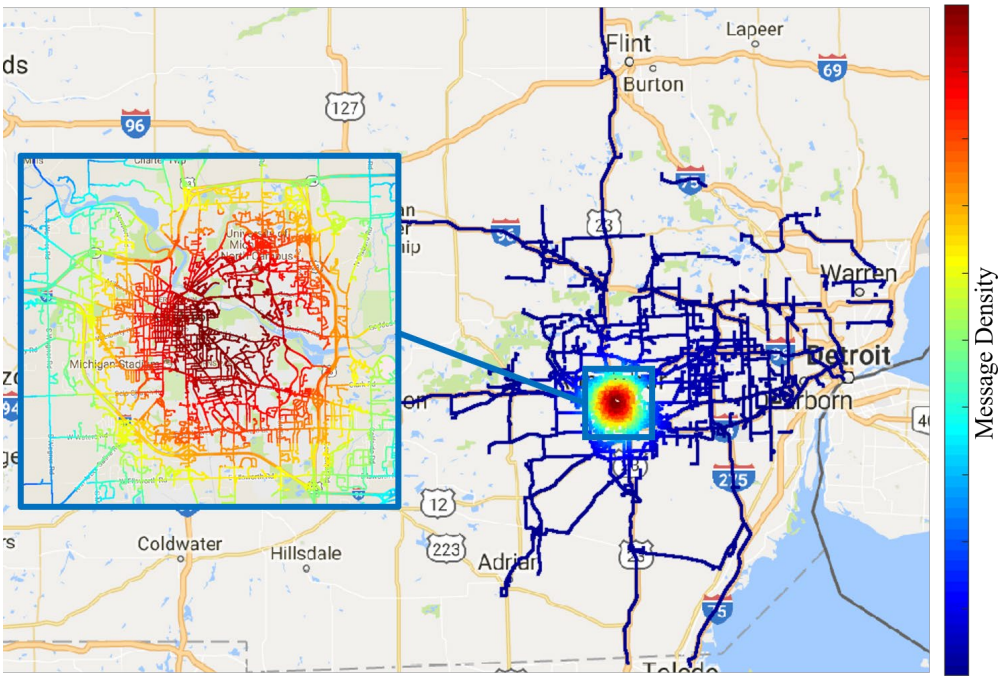


Fig. 1 Recorded vehicle location from Basic Safety Message (BSM) on May 1st, 2013 from the Safety Pilot Model Deployment (SPMD) databasev[5]

There are four types of vehicle equipment configurations, referred as Integrated Safety Device (ISD), Aftermarket

Safety Device (ASD), Retrofit Safety Device (RSD), and Vehicle Awareness Device (VAD) based on their ability to transmitting or receiving BSM, weight class, and equipment of cameras. All configurations can transmit BSM and VAD cannot receive BSM from other vehicles. The configurations are summarized in TABLE II. Among the 300 ASD vehicles, 98 were equipped with a Mobileye® camera, which records forward object, range, and lane tracking information.

TABLE II SPMD DSRC DEVICE SUMMARY

| Device | Rx | Weight Class | Quantity | Camera |
|---|---|---|---|---|
| ISD | Y | Light | 67 | Y |
| VAD | N | Light, Medium, Heavy Duty, Transit | 2,450 | N |
| ASD | Y | Light | 202 | N |
| | Y | Light | 98 | Y |
| RSD | Y | Heavy Duty, Transit | 19 | Y |

## 2.2 Sampled Dataset

### 2.2.1 Car-Following

The key variables for the car-following scenario include the range between the host vehicle and the leading vehicle $R_L$, range rate $\dot{R}_L$, speeds of the host vehicle $v$ and the leading vehicle $v_L$, longitudinal accelerations of the host vehicle $a$ and the leading vehicle $a_L$, lane positions of the host vehicle $Y$ and the leading vehicle $Y_L$. We use data from 98 sedans equipped with Mobileye® which provides a) relative position to the leading vehicle (range) and b) lane tracking measures compared with the lane delineation both from the painted boundary lines and the road edge. The range measurements error is up to 10% at 90m and 5% at 45m [31]. To ensure consistency of the dataset, we apply the following query criteria:

- $R_L(t) \in [0.1\ \text{m}, 90\ \text{m}]$
- Latitude between 41.0o and 44.5o
- Longitude between -88.2o and -82.0o
- No cut-in vehicles between the two vehicles
- No lane-change by either vehicle
- Duration longer than 50s, $\dot{R} \in$[-10m/s,10m/s], vehicle speed larger than 10 m/s

With the defined criteria, 161,009 car-following events were identified: 85,656 on local roads and 75,353 on highways. The sampled car-following events are shown in Fig. 2.

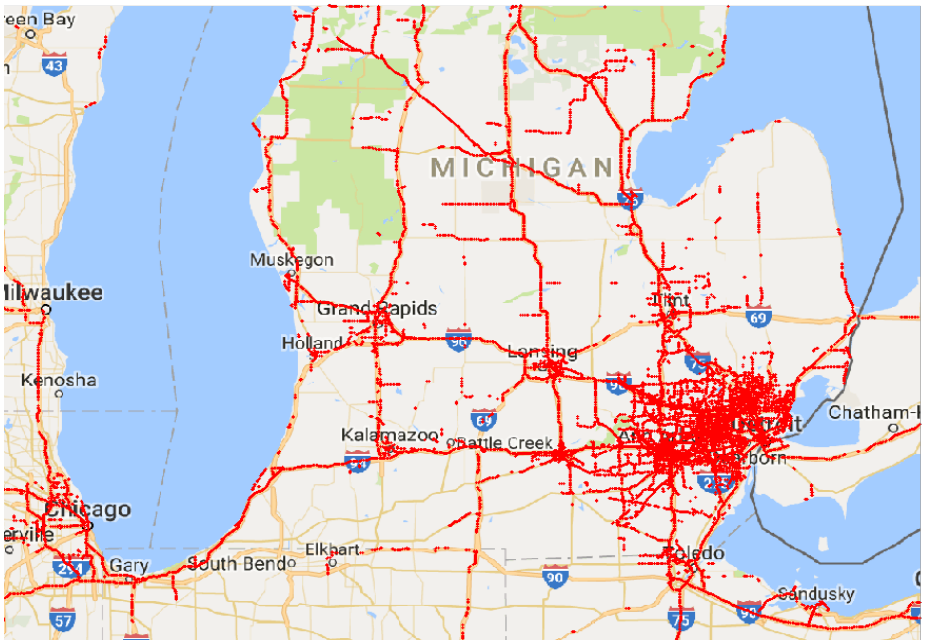


Fig. 1 Sampled car-following data location

### 2.2.2 Free-flow behavior

A Gaussian Mixture Model (GMM) based clustering algorithm is used to identify the free-flow condition from the data. The query criteria used for the trips are as follows:

- Trip duration longer than 10 minutes
- Trip length longer than 300 meters
- Trips inside the Ann Arbor area: latitude between 42.18° and 42.34°, and longitude between -83.85° and -83.55°

The results include 321,945 trips, which cover 3.7 million kilometers and more than 93,926 hours from 2,468 drivers. To match the trips to links (road sections), an algorithm developed by [32] is applied. The data covers 9,745 of the 11,506 road links in the Ann Arbor area.

### 2.2.3 Lane change

The lateral position of the lane change vehicle reported from the Mobileye® camera is used to identify lane-change events. As shown in Figure 3, the key lane-change variables include the initial range to the leading vehicle $R_{L0}$, initial time-to-collision $TTC_0$, initial vehicle speed of the host vehicle $v_0$, the maximum yaw rate $r_{max}$ during a lane-change, and the duration of lane-change $T$. The query criteria used for the lane-change scenario are as follows:

- Host vehicle is not changing lane
- Leading vehicle's lateral distance distance $d_{lat}$ to the host vehicle change from $d_{lat}(t_1) > 3m$ to $d_{lat}(t_2) < 0.3m$

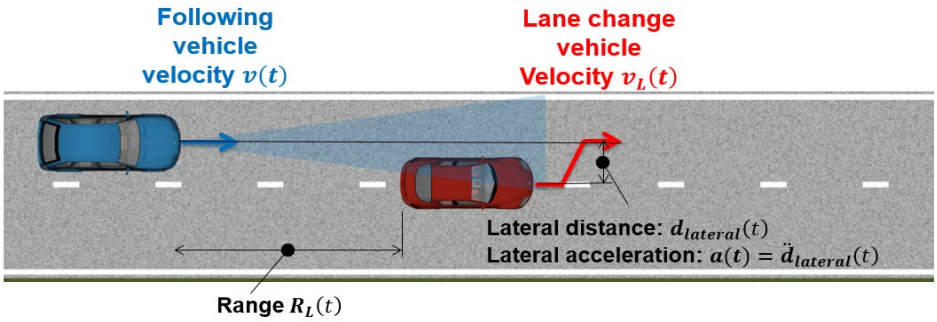


Fig. 3 Key variables extracted during a lane-change (cut-in) case

In total, 422,249 cut-in cases were obtained. In 179,401 (42.5%) cases, the leading vehicle change lane from left to right, and in 242,848 (57.5%) of the cases, the leading vehicle change lane from right to left. 332,283 (78.7%) cases happen on local roads, and 89,966 (21.3%) cases happen on highways.

## 3. Results and Discussion

### 3.1 Control actions

#### 3.1.1 Longitudinal Acceleration and Deceleration

Longitudinal acceleration and deceleration characterize how decisive a vehicle is, and is an important behavior we study. On local roads, the distribution has a longer tail compared with that on highways. The probability density function (PDF) longitudinal acceleration distribution of a selected driver is shown in Fig. 4. The distribution is asymmetric due to the difference in the powertrain acceleration and deceleration capabilities as well as driver's performance difference in acceleration and braking events. In the following, we refer to deceleration as acceleration with brake applied, and acceleration as acceleration with throttle applied.

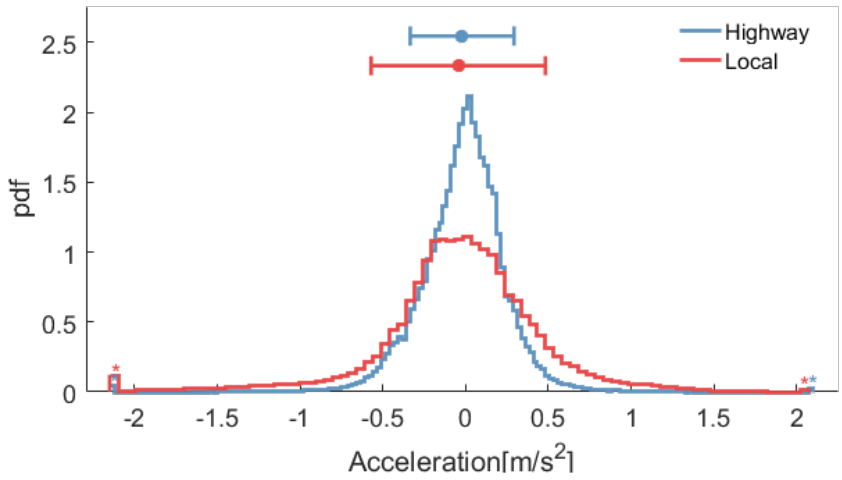


Fig. 2 Longitudinal Acceleration Distribution for a Single Driver During Car-Following for Highway and Local Driving

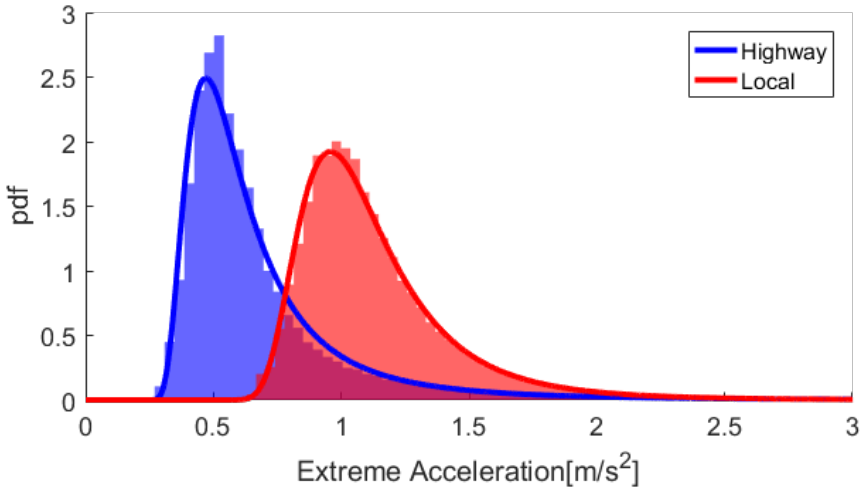


Fig. 3 Extreme acceleration distribution for all drivers

For each driver, we define deceleration stronger than 2.5% percentile as extreme deceleration and acceleration stronger than 97.5% percentile as extreme acceleration. The extreme acceleration $a_{lim,a}$ and deceleration $a_{lim,d}$ of all drivers are shown in Fig. 5 and Fig. 6, respectively. The distributions are fitted with a Generalized Extreme Value (GEV) distribution model which is a common choice to model the maxima of finite sequences of random variables [33]. Since extreme deceleration is defined as minimal acceleration instead of the maxima, we fit negation of extreme deceleration. The parameters of the GEV distribution include shape parameter k, scale parameter σ and location parameter μ, the probability function is shown below

$$f(x\,|\,k,\mu,\sigma)=\begin{cases}\dfrac{1}{\sigma}\exp\left(-\left(1+\dfrac{k(x-\mu)}{\sigma}\right)^{-\frac{1}{k}}\right)\left(1+\dfrac{k(x-\mu)}{\sigma}\right)^{-1-\frac{1}{k}} & k\neq 0\\ \dfrac{1}{\sigma}\exp\left(-\exp\left(-\dfrac{x-\mu}{\sigma}\right)-\dfrac{x-\mu}{\sigma}\right) & k=0\end{cases} \quad (1)$$

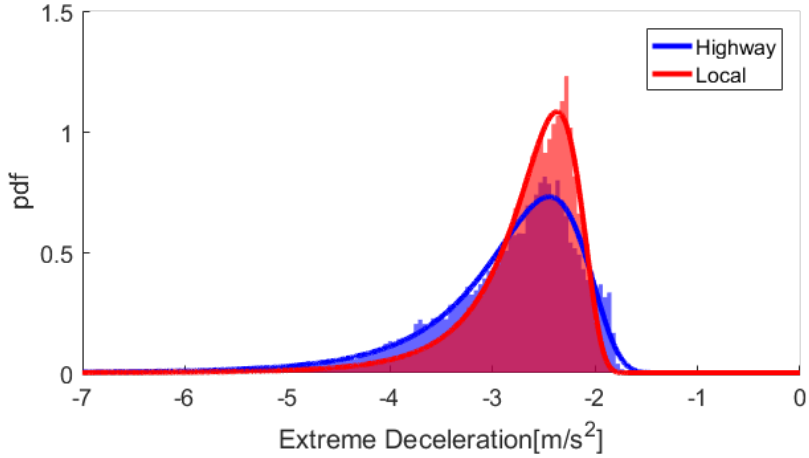

Fig. 4 Extreme deceleration distribution for all drivers

The parameters are summarized in TABLE III. Human drivers have higher acceleration levels on local roads than on highways, with average acceleration limit 0.72 m/s$^2$ for highway and 1.19 m/s$^2$ for local roads. The mean deceleration limit for highway and local car-following are close, with -2.81 m/s$^2$ for highway and -2.64 m/s$^2$ for local roads. However, the tail for highway deceleration is longer than local driving.

TABLE III ACCELERATION AND DECELERATION LIMIT GEV DISTRIBUTION PARAMETERS FOR HIGHWAY AND LOCAL CAR-FOLLOWING

| Scenario | | $k$ | $\sigma$ | $\mu$ |
|---|---|---|---|---|
| Highway | $a_{lim,a}$ | 0.3711 | 0.1628 | 0.5314 |
| | $-a_{lim,d}$ | 0.1669 | 0.4722 | 2.4461 |
| Local | $a_{lim,a}$ | 0.1426 | 0.1930 | 1.0457 |
| | $-a_{lim,d}$ | 0.1649 | 0.3289 | 2.3865 |

### 3.1.2 Maximum Yaw rate During Lane-Changes

To prevent a robotic vehicle executing a lane-change too aggressively, it is important to learn human lane-change maximum yaw rate $r_{max}$. In this section, the distributions of $r_{max}$ of local roads and highway are analyzed. The yaw rate of lane-change vehicle is estimated with Kalman Filter using the time series of lateral velocity of the lane-change vehicles. Assuming the initial lateral acceleration of each lane-change event is zero, we calculate the lateral acceleration time series with discrete Kalman Filter following [34] and [35]. The lateral dyanmics is approximated as

$$\begin{aligned}\begin{bmatrix} v_y^{k+1} \\ a_y^{k+1} \end{bmatrix} &= \begin{bmatrix} 1 & dt \\ 0 & 1 \end{bmatrix}\begin{bmatrix} v_y^{k} \\ a_y^{k} \end{bmatrix} + \omega_k = A\chi_k + \omega_k, \omega_k \sim N(0,Q) \\ v_y^k &= \begin{bmatrix} 1 & 0 \end{bmatrix}\begin{bmatrix} v_y^{k} \\ a_y^{k} \end{bmatrix} + \vartheta_k = C\chi_k + \vartheta_k, \vartheta_k \sim N(0,R)\end{aligned} \quad (2)$$

where $v_y$ is the lateral velocity and the $a_y$ is the lateral acceleration. Denote the state as $x$, covatiacne of state as $P$, system dyanimcs matrix as $A$ and observation matrix as $C$, the state can be predicted from the dynamics model and covariance can be predicted from Gaussian approximaion of dynamics and observation noise

$$\begin{aligned} x_{k+1|k} &= Ax_{k|k} \\ P_{k+1|k} &= AP_{k|k}A^T + R \end{aligned} \quad (2)(3)$$

where $x_{k+1|k}$ and $P_{k+1|k}$ are predicted state and state covariance given observation at time $k$, and $x_{k|k}$ and $P_{k|k}$ are estimated state and state covatiance at time $k$. Given new obserrvation at time $k+1$, the estimated state and covariance can be updated as

$$\begin{aligned} \Delta_{k+1} &= CP_{k+1|k}C^T + Q \\ x_{k+1|k+1} &= x_{k+1|k} + P_{k+1|k}C^T\Delta_{k+1}^{-1}(v_y^{k+1} - C\chi_{k+1|k}) \\ P_{k+1|k+1} &= P_{k+1|k} - P_{k+1|k}C^T\Delta_{k+1}^{-1}CP_{k+1|k}^T \end{aligned} \quad (4)(5)(6)$$

After calculating the lateral acceleration time series, we derive the yaw rate by

$$r = \frac{a_y}{v_x} \quad (7)$$

where $v_x$ is the longitudial speed and $r$ is the yaw rate. Maximum yaw rate of all events are fitted with GEV distirbution, the results are shown in Fig. 7 and the model parameters are summerized in TABLE IV. As shown in Fig. 7, the average maximum yaw rate of the local lane-change (1.4 deg/s) is much higher than the highway lane-change (0.6 deg/s) and the local lane-change maximum yaw rate has a longer tail.

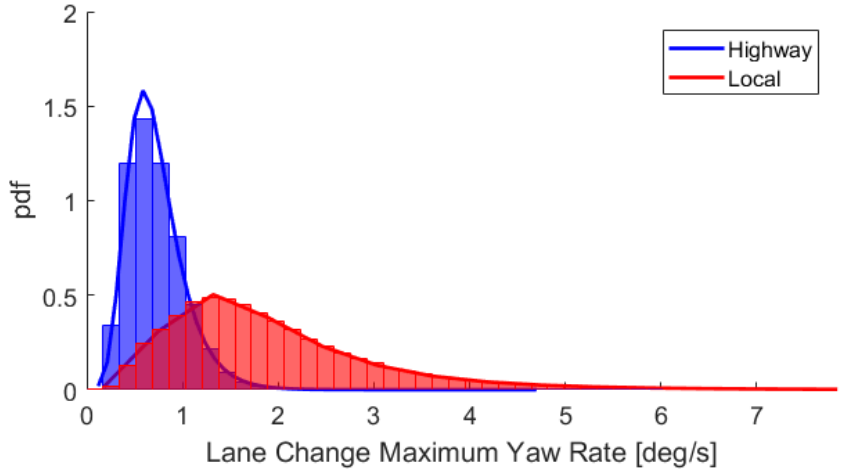


Fig. 5 Lane-Change Maximum Yaw Rate Distribution

TABLE IV MAXIMUM YAW RATE GEV DISTRIBUTION PARAMETERS FOR HIGHWAY AND LOCAL LANE-CHANGE

| Scenario | | $k$ | $\sigma$ | $\mu$ |
|---|---|---|---|---|
| Highway | $r_{max}$ | -0.0083 | 0.2325 | 0.5900 |
| Local | $r_{max}$ | 0.1525 | 0.7381 | 1.3953 |

## 3.2 Free flow behaviors

The free flow driving behavior was studied extensively in the literature [36]. Measurement data from roadside sensors show that the traffic flow demonstrates a multimodal behavior, which was commonly described by a three-phase traffic theory: free flow, synchronized flow, and wide-moving jam. The latter two phases are associated with congested traffic. Based on this theory, we use the Gaussian Mixture Model (GMM) [37] following previous work in link travel time estimation [38] with 3 components to identify the free flow and congested behaviors.

$$f(x \mid \pi_1,\ldots,_{k'},\theta_1,\ldots,k) = \sum_{k=1}^{3} \pi_k f_k(x \mid \theta_k) \quad (8)$$

where $\pi_k$ is weighting parameters, and $f_k(x|\theta_k)$ is the multivariate normal probability density function of each

component, $\theta_k$ is the collection of model parameter of each component, which includes mean and covariance matrix. The model assumes that the congestion status can be viewed as a discrete random variable, and the vehicle speed is a random variable conditional on the congestion status. Samples of local and highway speed models for one road section are shown in Fig. 8 and Fig. 9.

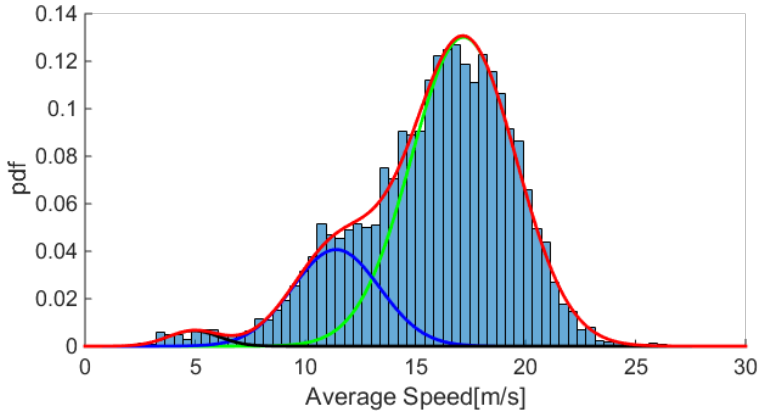


Fig. 6 Speed histogram and GMM fitting for one local road section with a speed limit at 17.88 m/s (40 mph)

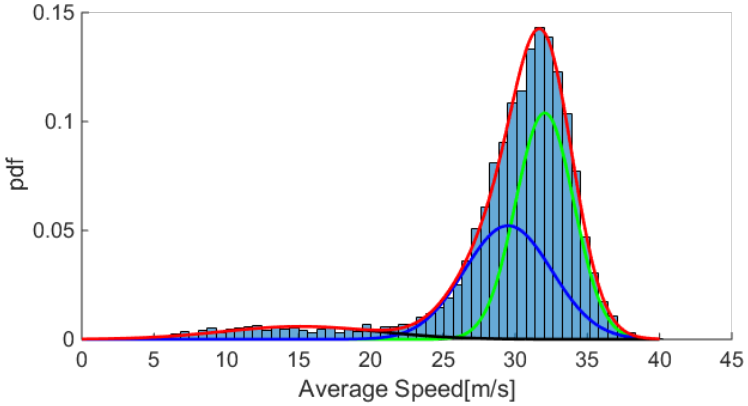


Fig. 7 Speed histogram and GMM fitting for one highway road section with a speed limit 31.29 m/s (70 mph)

We use the component with the highest mean value for each link to estimate the free flow behavior. The measured free-flow speed compared with the posted speed limits are shown in Fig. 10 and Fig. 11, where the observed free flow speed of the road links vs. speed limits shown in a box plot and posted speed limit shown in a solid line. As shown in the figures, the observed free-flow speed is significantly higher than the posted speed limits on the highways. According to the Highway Capacity Manual [39], the base free-flow speed is estimated to be 2.2 m/s (5 mph) above the posted speed limit. However, as shown in Fig. 10, for highway links with lower speed limits, the HCM estimated base free-flow speeds are much lower than the measured values. This could pose a dilemma for robot drivers—if the robots are programmed to follow the speed limit, they will drive much slower than human driven vehicles, especially on highways with slower posted speed limit (e.g., 45 mph). For local roads, the mean free-flow speeds are very close to the posted speed limits, with a correlation coefficient of 0.99.

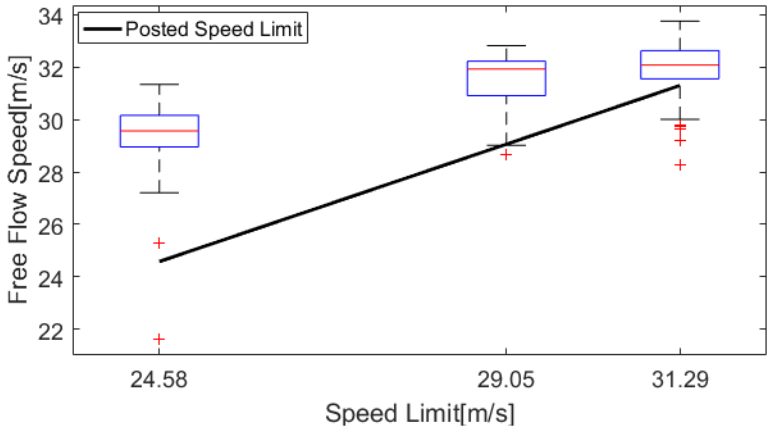


Fig. 8 Free Flow Speed vs. Posted Speed Limit for Highways

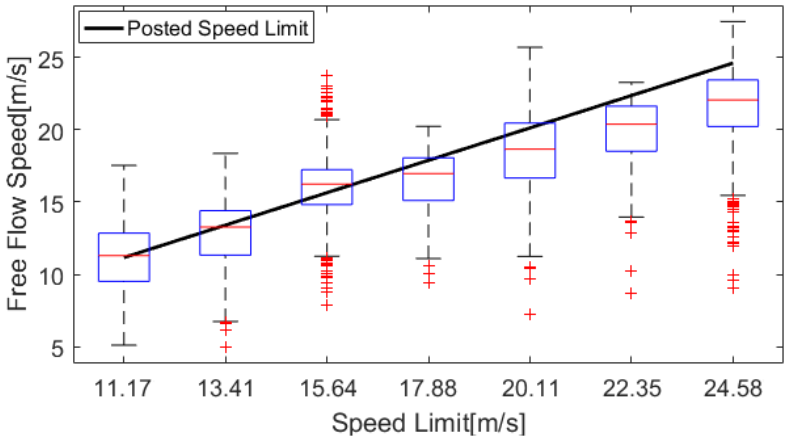


Fig. 9 Free Flow Speed vs. Posted Speed Limit for Local Roads

## 3.3 Car-following behavior

### 3.3.1 Distance to the Lead Vehicle

The relative position from a host vehicle to the lead vehicle can be defined by the time headway, which is range divided by the speed of the host vehicle. The constant time headway policy is frequently used as a safe driving practice for human drivers and for Adaptive Cruise Control designs. Two key statistic parameters are the average time headway and minimum time headway. For human drivers, the lognormal function was found to fit their time headway distribution well [40]. The sample time headway distribution of a single driver for both highway and local car-following events are shown in Fig. 12. As shown in the histograms, the sampled driver tends to keep a longer time headway on local roads, and the variance is larger, compared with the behavior on highways.

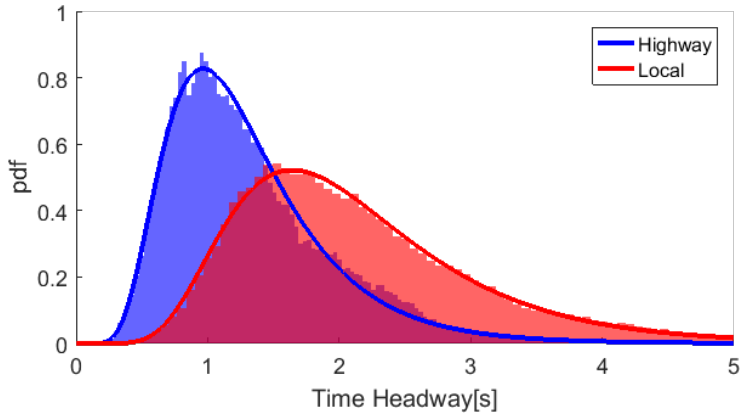


Fig. 10 Time Headway Distribution and Lognormal Model for Single Driver in Car-Following Scenario for Highway and Local Driving

To model the time headway distribution for the entire driver population, the mean time headway for each driver is calculated and plotted in Fig. 13. The distribution is fitted using a lognormal distribution function, and the parameters are summarized in TABLE V. The mean car-following time headway for highway driving is 1.42 s. Our highway results agree with previous studies such as [41] which concluded that car-following time headway for highway is between 1.3 s and 1.6 s, which correspond to 25% and 75% percentiles of our model. The 25% and 75% percentiles of local road sections are 1.77 s and 2.33 s. From the histograms, time headway for local roads is longer than that of highways, which has a median of 2.03 s and an average of 2.07 s.

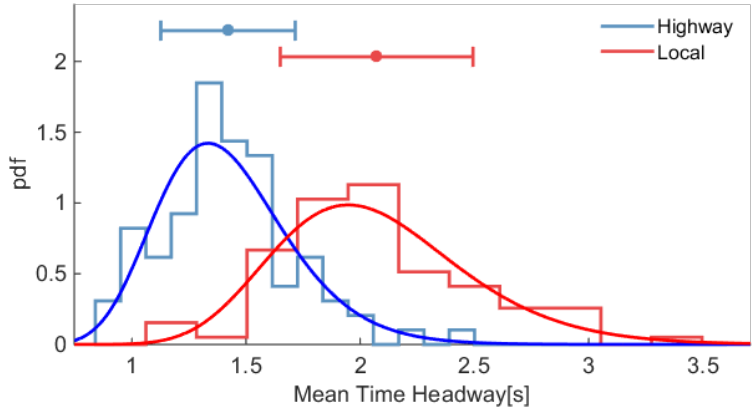


Fig. 11 Mean time headway distribution of all drivers for highway and local car-following events

TABLE V MEAN CAR-FOLLOWING TIME HEADWAY LOGNORMAL DISTRIBUTION PARAMETERS AND PERCENTILE

| Scenario | Mean [$s$] | Variance [$s^2$] | Percentile [$s$] | | |
|---|---|---|---|---|---|
| | | | 25% | 50% | 75% |
| Highway | 1.42 | 0.08 | 1.21 | 1.39 | 1.60 |
| Local | 2.07 | 0.18 | 1.77 | 2.03 | 2.33 |

The minimum car-following distance is also calculated for all drivers. For each driver, the extreme time

headway is defined as time headway shorter than 2.5% percentile of the distribution of that driver. The extreme time headway of all drivers are shown in Fig. 14. The random variables are characterized with GEV distributions, and the parameters are summarized in TABLE VI. The extreme time headway on highways is 0.44 s, shorter than the 0.80 s for local roads. The standard deviation is 0.021 s on highways, lower than that that of the for local roads (0.071 s).

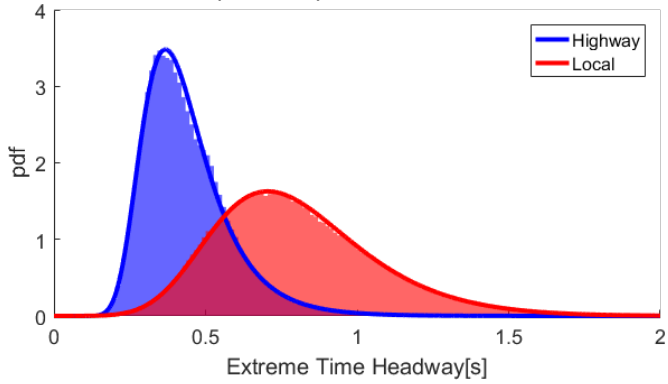


Fig. 12 Extreme time headway distribution for all drivers

TABLE VI TIME HEADWAY LIMIT GEV DISTRIBUTION PARAMETER FOR HIGHWAY AND LOCAL CAR-FOLLOWING

| Scenario | | $k$ | $\sigma$ | $\mu$ |
|---|---|---|---|---|
| Highway | $Th_{lim}$ | 0.0415 | 0.1058 | 0.3720 |
| Local | $Th_{lim}$ | -0.0737 | 0.2267 | 0.6880 |

In addition to time headway, another variable commonly used to characterize driving is time to collision (TTC), which is defined as the ratio between range and the absolute value of range rate. Since the closing-in process is of interest, we only analysis the cases when range rate is negative. The "starting-to-brake TTC" is the TCC when the human drivers started to apply the brake, for both highway and local car-following events, are shown in Fig. 15. The distributions are again characterized with a GEV distribution. The model parameters are obtained from maximum likelihood estimation and are summarized in TABLE VII. The results indicate that the starting-to-brake TTC for highway and local car-following cases are similar, with the average value at around 22 s, while the mode is at 12 seconds.

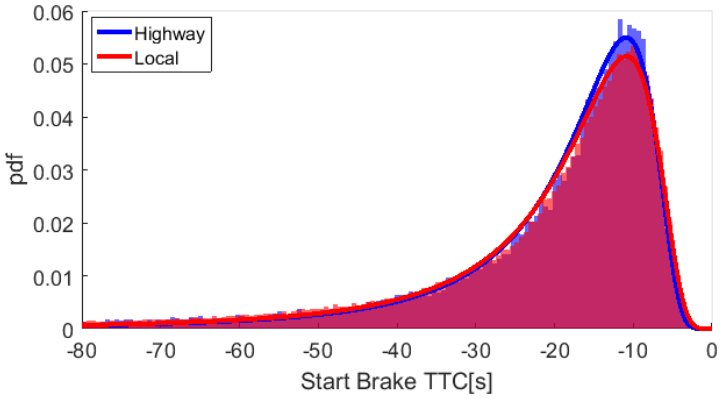


Fig. 13 Starting-to-brake TTC of highway and local car-following events

TABLE VII START-TO-BRAKE TTC GEV DISTRIBUTION PARAMETER FOR HIGHWAY AND LOCAL CAR-FOLLOWING

| Scenario | | $k$ | $\sigma$ | $\mu$ |
|---|---|---|---|---|
| Highway | $\lvert TTC_{lim}\rvert$ | 0.4006 | 7.1869 | 13.1760 |
| Local | $\lvert TTC_{lim}\rvert$ | 0.3989 | 7.6780 | 13.2650 |

### 3.3.2 Dynamic Response to the Lead Vehicle

The dynamic response of human drivers to the lead vehicle can be understood by the correlation between acceleration (the control action) to the range and range rate (the vehicle states), e.g., following the driver model proposed by [40]. In this model, both correlations are modeled as a function of range $R_L$. The acceleration can be expressed as

$$a_d = K_D(R_L)\dot{R}_L + K_P(R_L)(R_L - Th_d \cdot v) \qquad (2)$$

where $K_D$ is the control gain for the range rate, and $K_P$ is the control gain for the range, $Th_d$ is the desired time headway to the lead vehicle. The sample joint distributions for range, range rate and acceleration of a single driver are shown in Fig. 16 and Fig. 17. At longer range, the variance of acceleration decreases, indicating human drivers are less sensitive. The correlations are modeled as a 3rd order polynomials in range. The parameters are estimated using robust least square with a bisquare function as regularization weights. [42] With this algorithm, the parameter estimation is more robust against outliers. For each driver, the correlation polynomials are estimated, and then the results for all drivers are used to construct the model of correlation parameters. The joint distribution for the correlations and range are shown in Fig. 18. It can be seen that the drivers use higher feedback gains when they are closer to the lead vehicle. The GEV distribution is used to model the random variable to capture the asymmetricity [40].

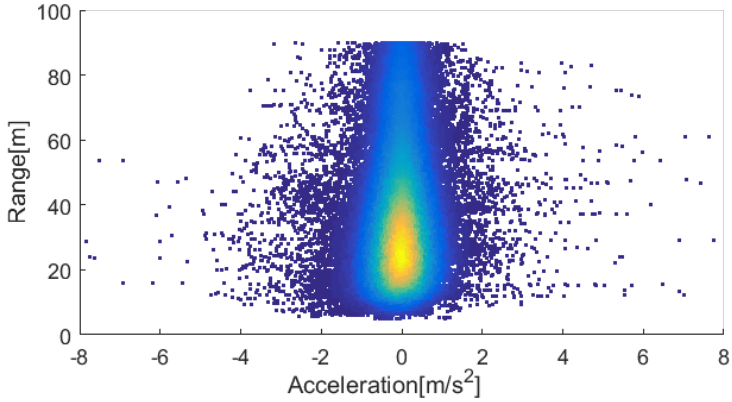


Fig. 14 Joint distribution of acceleration and range of a single driver highway car-following scenario

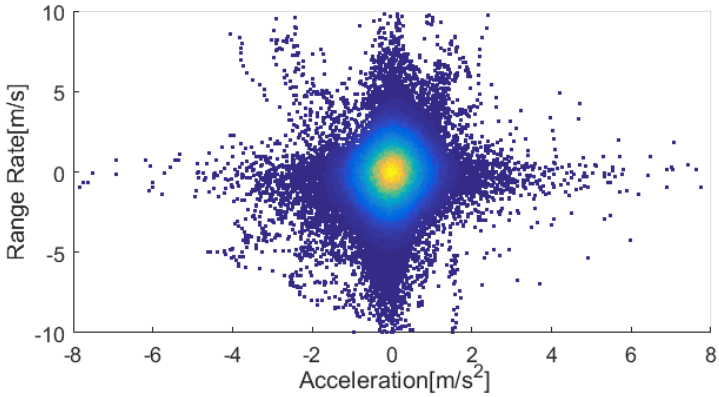


Fig. 15 Joint distribution of acceleration and range rate of a single driver highway car-following scenario

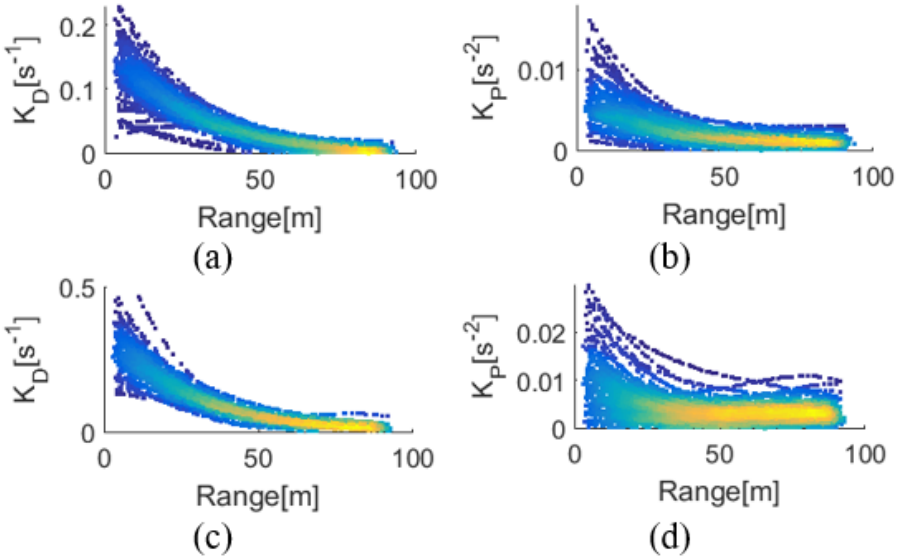


Fig. 16 Joint distribution of correlation and range for different scenarios: (a) $K_D$ for highway; (b) $K_P$ for highway; (c) $K_D$ for local; (d) $K_D$ for local

With distribution parameters estimated for all car-following cases, the population mean of the correlation function and the percentiles are computed. The mean correlation and 25% and 75% percentiles at different car-following ranges are shown in Fig. 19 and Fig. 20.

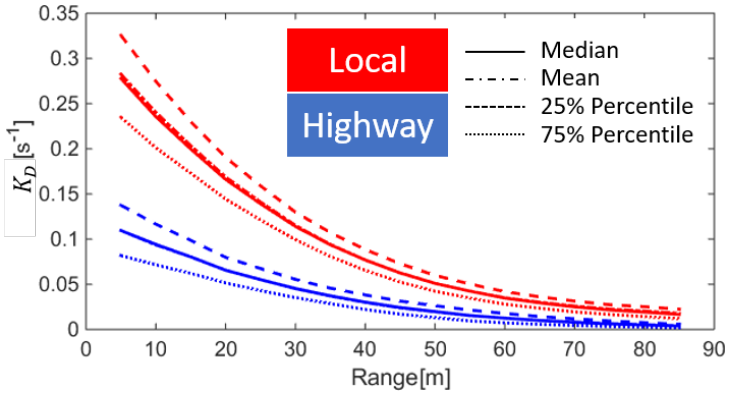


Fig. 17 Mean correlation between acceleration and range rate at different ranges for highway and local car-following scenarios

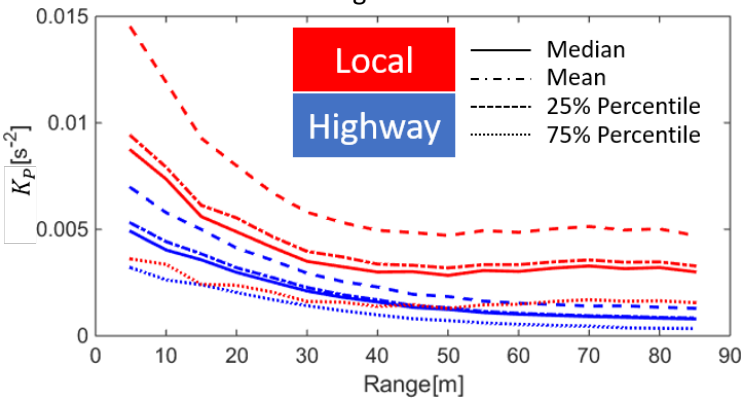


Fig. 18 Mean correlation between acceleration and range error at different ranges for highway and local car-following scenarios

## 3.4 Lane-change behavior

### 3.4.1 Initial Longitudinal Distance of Lane-Change

The initial following vehicle time headway of a lane-change maneuver is an important parameter to characterize cut-in behaviors. Human drivers examine the available adjacent gaps (represented by time headway) to decide whether to change lane [43]. Therefore, it is crucial to understand how human drivers accept the gap for lane-changes.

For the local data, it can be seen from Fig. 21 that the joint distribution of time headway reciprocal and range rate has one component and time headway is independent with range rate. Therefore, we use GEV to model time headway reciprocal with the hypothesis that the initial time headway corresponds to the minimal accepted gap for human driver cut-in and we use Normal distribution to model the range rate. The PDF then can be expressed as

$$f(x_1, x_2|k_1, \sigma_1, \mu_1, \mu_2, \sigma_2) = f_{GEV}(x_1|k_1, \sigma_1, \mu_1) f_N(x_2|\mu_2, \sigma_2) \quad (3)$$

where $f_{GEV}$ is the PDF of GEV distribution, $f_N$ is the PDF of Normal distribution, $x_1$ is time headway reciprocal and $x_2$ is range rate. The parameters are shown in TABLE VIII.

Fig. 19 Joint Distribution of Time Headway Reciprocal and Range Rate of Local Lane-Change

For the highway data, it can be seen from the joint histogram of time headway reciprocal and range rate in Fig. 22 that the data follows a two-component distribution. This phenomenon may due to the purpose of lane-changes on highway. Our hypothesis is that the right component is due to mandatory lane-change s such as merging into a platoon where the time headway of the following vehicle is relatively small to the cut-in vehicle. And the left component represents the normal discretionary lane-changes. Therefore, for the right component, we use multivariate Normal distribution to fit the data, and for the left component, we use the same model as local scenario. The probability density function then can be expressed as

$$f(x_1, x_2|k_1, \sigma_1, \mu_1, \mu_2, \sigma_2, \mu_3, \sigma_3, \pi) = \pi f_{GEV}(x_1|k_1, \sigma_1, \mu_1) f_N(x_2|\mu_2, \sigma_2) + (1-\pi) f_{MN}(x_1, x_2|\mu_3, \sigma_3) \quad (4)$$

where $f_{GEV}$ is the PDF of GEV distribution, $f_N$ is the PDF of normal distribution, $f_{MN}$ is the PDF of multivariate Normal distribution, $\pi$ is the mixture weight, $x_1$ represents time headway reciprocal and $x_2$ represents range rate. The parameters are shown in TABLE VIII. Verifying the lane-change classification hypothesis using camera videos recorded by Mobileye is left for future work.

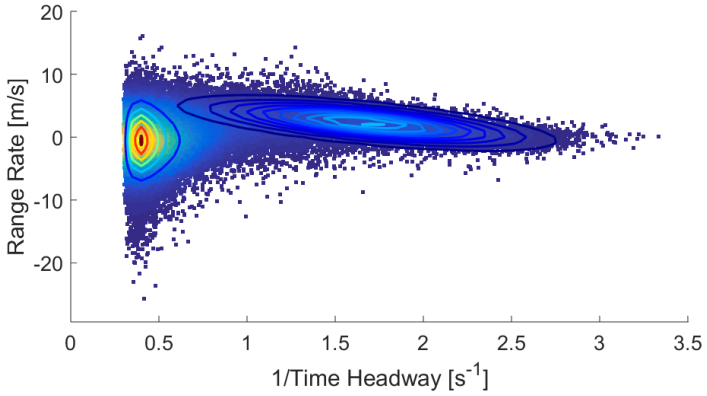


Fig. 20 Joint Distribution of Time Headway Reciprocal and Range Rate of Local Lane-Change

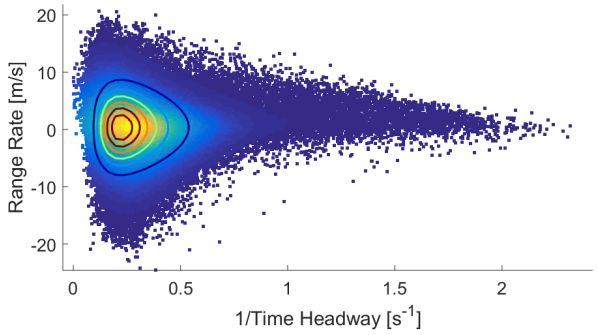


Fig. 21 Joint Distribution of Time Headway Reciprocal and Range Rate of Highway Lane-Change

TABLE VIII TIME HEADWAY RECIPROCAL VS. RANGE RATE JOINT DISTRIBUTION PARAMETERS FOR HIGHWAY AND LOCAL LANE-CHANGE

| | | | | |
|---|---|---|---|---|
| Highway | $f_{GEV}$ | $k_1$ 0.3388 | $\sigma_1$ 0.0731 | $\mu_1$ 0.4085 |
| | $f_N$ | $\mu_2$ -0.5426 | $\sigma_2$ 3.3230 | |
| $\pi$ =0.78 | $f_{MN}$ | $\mu_3$ [1.68,2.23] | $\sigma_3$ $\begin{bmatrix} 0.25 & -0.65 \\ -0.65 & 4.13 \end{bmatrix}$ | |
| Local | $f_{GEV}$ | $k_1$ 0.1589 | $\sigma_1$ 0.1013 | $\mu_1$ 0.2344 |
| | $f_N$ | $\mu_2$ 0.3478 | $\sigma_2$ 4.2381 | |

3.4.2 Initial Time to Collision (TTC) of Lane-Change

As in [44], the initial TTC reciprocal is analyzed. Positive TTC represents cases when the following vehicle is catching up to the leading lane-change vehicle. The higher initial TTC reciprocal, the riskier the lane-change is. We use double exponential distribution to capture both negative and positive TTC reciprocal following [44]. The PDF is defined as

$$f(TTC) = \frac{\lambda}{2}\exp(-\lambda|TTC - \mu|) \qquad (12)$$

where $\lambda$ is shape parameter, and $\mu$ is mean value parameter. And for positive initial TTC reciprocal cases, the data is modeled using exponential distribution following [44], with the PDF defined as

$$f(TTC) = \frac{1}{\mu}\exp\left(-\frac{TTC}{\mu}\right) \qquad (5)$$

where $\mu$ is the mean parameter. The model results are shown in Fig. 23 and Fig. 24, and the model parameters are shown in TABLE IX and TABLE X for initial TTC and positive initial TTC respectively.

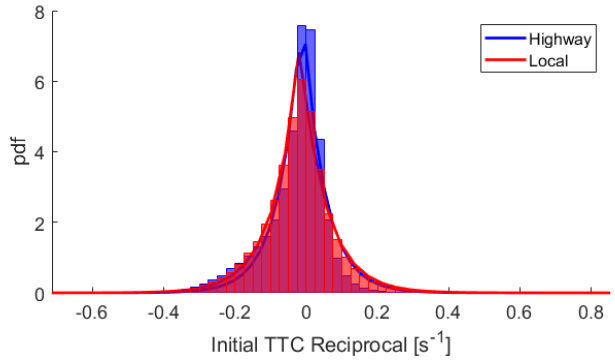


Fig. 22 Lane-Change Initial TTC Reciprocal Distribution

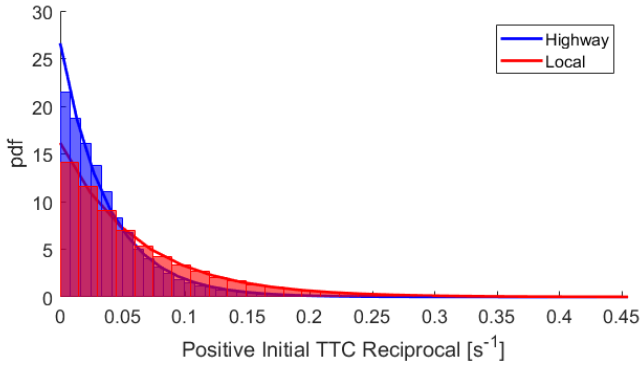


Fig. 23 Positive Initial TTC Reciprocal Distribution

TABLE IX INITIAL TTC RECIPROCAL DOUBLE EXPONENTIAL DISTRIBUTION PARAMETERS FOR HIGHWAY AND LOCAL LANE-CHANGE

| Scenario | | $\lambda$ | $\mu$ |
|---|---|---|---|
| Highway | $TTC_0^{-1}$ | 16.5370 | -0.0120 |
| Local | $TTC_0^{-1}$ | 14.0112 | -0.0185 |

TABLE X POSITIVE INITIAL TTC RECIPROCAL EXPONENTIAL DISTRIBUTION PARAMETERS FOR HIGHWAY AND LOCAL LANE-CHANGE

| Scenario | | | $\mu$ | |
|---|---|---|---|---|
| Highway | $+TTC_0^{-1}$ | | 0.0376 | |
| Local | $+TTC_0^{-1}$ | | 0.0619 | |
| Percentile | 10% | 30% | 70% | 90% |
| Highway | 1/219.7 | 1/68.0 | 1/22.5 | 1/12.1 |
| Local | 1/148.5 | 1/45.0 | 1/13.4 | 1/6.95 |

### 3.4.3 Duration of Lane-Change

The duration of lane-change is another important feature indicating how aggressive the lane-change is. The lane-change duration $T$ is modeled with log normal distribution following [29], with the PDF defined as

$$f(T) = \frac{1}{T\sigma\sqrt{2\pi}} \exp\left(-\frac{(\ln T - \mu)^2}{2\sigma^2}\right) \qquad (6)$$

where $\mu$ is the mean of logarithmic values and σ is the standard deviation of logarithmic values. As shown in Fig. 25, the mean duration of lane-change in highway (4.3s) is longer than the duration of lane-change in local road (2.0s). The distribution parameters and percentiles are shown in TABLE XI.

TABLE XI DURATION GEV DISTRIBUTION PARAMETERS FOR HIGHWAY AND LOCAL LANE-CHANGE

| Scenario | | σ | μ |
|---|---|---|---|
| Highway | T | 0.6569 | 1.6842 |
| Local | T | 0.6910 | 1.0483 |

| Percentile | 10% | 30% | 70% | 90% |
|---|---|---|---|---|
| Highway | 2.2 | 3.6 | 8.1 | 13.1 |
| Local | 1.2 | 1.8 | 4.0 | 7.8 |

## 4. Conclusions and Future Work

In this paper we present the key parameters of human driver behaviors in three driving scenarios: free-flow, car-following and lane-change, obtained from a naturalistic driving database.

Our results can be used to design control algorithm of automated vehicle so that it is compatible to local driving culture. The results can also be used to develop driving simulation software to simulate human-driven vehicles. Our next step includes developing automated vehicle based on the parameters and validate the functions in testing facilities such as Mcity [45]. Also, since data from SPMD is used for the analysis, using naturalistic database from other test sites would be helpful to analyze the extrapolability of our model.

## 5. References

[1] D. J. Fagnant and K. Kockelman, "Preparing a nation for autonomous vehicles: Opportunities, barriers and policy recommendations," *Transp. Res. Part A Policy Pract.*, vol. 77, pp. 167–181, 2015.
[2] T. Litman, "Autonomous Vehicle Implementation Predictions: Implications for Transport Planning," *Transp. Res. Board Annu. Meet.*, no. 2014, pp. 36–42, 2014.
[3] F. M. Favarò, N. Nader, S. O. Eurich, M. Tripp, and N. Varadaraju, "Examining accident reports involving autonomous vehicles in California," *PLoS One*, vol. 12, no. 9, p. e0184952, 2017.
[4] "Report of Traffic Collision Involving an Autonomous Vehicle (OL 316)." [Online]. Available: https://www.dmv.ca.gov/portal/dmv/detail/vr/autonomous/autonomousveh_ol316+. [Accessed: 03-Jul-2018].
[5] D. Bezzina and J. Sayer, "Safety pilot model deployment: Test conductor team report," *Rep. No. DOT HS*, vol. 812, no. June, p. 171, 2014.
[6] J. C. Gerdes and J. K. Hedrick, "Vehicle speed and spacing control via coordinated throttle and brake actuation," *Control Eng. Pract.*, vol. 5, no. 11, pp. 1607–1614, 1997.
[7] X.-Y. Lu, H.-S. Tan, S. Shladover, and J. K. Hedrick, "Nonlinear Longitudinal Controller Implementation and Comparison for Automated Cars," *Journal of Dynamic Systems, Measurement, and Control*, vol. 123. p. 161, 2001.
[8] P. Ioannou and Z. Xu, "Throttle and Brake Control Systems for Automatic Vehicle Following," *J. Intell. Transp. Syst.*, vol. 1, no. 4, pp. 345–377, 1994.
[9] C.-Y. Liang and H. Peng, "String stability analysis of adaptive cruise controlled vehicles," *JSME Int. J. Ser. C*, vol. 43, no. 3, pp. 671–677, 2000.
[10] J. Zhou and H. Peng, "Range policy of adaptive cruise control vehicles for improved flow stability and string stability," *Intell. Transp. Syst. IEEE Trans.*, vol. 6, no. 2, pp. 229–237, 2005.
[11] J. Zhang and P. A. Ioannou, "Longitudinal control of heavy trucks in mixed traffic: Environmental and fuel economy considerations," *IEEE Trans. Intell. Transp. Syst.*, vol. 7, no. 1, pp. 92–104, 2006.
[12] I. Copyright © 2010 by the Institute of Electrical and Electronics Engineers, *802.11P-2010*. 2010.
[13] J. Ploeg, A. F. A. Serrarens, and G. J. Heijenk, "Connect & Drive: design and evaluation of cooperative adaptive cruise control for congestion reduction," *J. Mod. Transp.*, vol. 19, no. 3, pp. 207–213, 2011.
[14] J. Ge and G. Orosz, "Optimal control of connected vehicle systems," in *Decision and Control (CDC), 2014 IEEE 53rd Annual Conference on*, 2014, pp. 4107–4112.
[15] A. Vahidi and A. Eskandarian, "Research advances in intelligent collision avoidance and adaptive cruise control," *Intell. Transp. Syst. IEEE Trans.*, vol. 4, no. 3, pp. 143–153, 2003.
[16] T. Sauer and O. Tschernoster, "The BMW Active Cruise Control ACC," *SAE Int.*, p. 9, 2000.
[17] C. Hatipoglu, Ü. Özguner, and K. A. Redmill, "Automated lane change controller design," *IEEE Trans. Intell. Transp. Syst.*, vol. 4, no. 1, pp. 13–22, 2003.
[18] S. Ammoun, F. Nashashibi, and C. Laurgeau, "An analysis of the lane changing manoeuvre on roads : the contribution of inter-vehicle cooperation via communication," *2007 IEEE Intell. Veh. Symp.*, pp. 1095–1100, 2007.
[19] A. Kondyli and L. Elefteriadou, "Modeling Driver Behavior at Freeway-Ramp Merges," *Transp. Res. Rec. J. Transp. Res. Board*, vol. 2249, no. 2249, pp. 29–37, 2011.
[20] L. Guo, P. S. Ge, M. Yue, and Y. B. Zhao, "Lane changing trajectory planning and tracking controller design for intelligent vehicle running on curved road," *Math. Probl. Eng.*, vol. 2014, 2014.
[21] Y. Zhang and P. A. Ioannou, "Combined Variable Speed Limit and Lane Change Control for Highway Traffic," *IEEE Trans. Intell. Transp. Syst.*, vol. PP, no. 99, pp. 1–12, 2016.
[22] F. Paul, H. Jim, M. L. Buonarosam, B. Zevi, S. E. Bogard, M. R. Hagan, J. R. Sayer, and R. D. Ervin, "Intelligent cruise control field operational test. Final report. Volume I: Technical report," 1998.
[23] M. Brackstone and M. McDonald, "Driver headway: How close is too close on a motorway?," *Ergonomics*, vol. 50, no. 8, pp. 1183–1195, 2007.
[24] C. Miyajima, Y. Nishiwaki, K. Ozawa, T. Wakita, K. Itou, K. Takeda, and F. Itakura, "Driver modeling based on driving behavior and its evaluation in driver identification," *Proc. IEEE*, vol. 95, no. 2, pp. 427–437, 2007.
[25] G. F. Newell, "A simplified car-following theory: A lower order model," *Transp. Res. Part B Methodol.*, vol. 36, no. 3, pp. 195–205, 2002.
[26] S. A. Birrell, M. Fowkes, and P. A. Jennings, "Effect of using an in-vehicle smart driving aid on real-world driver performance," *IEEE Trans. Intell. Transp. Syst.*, vol. 15, no. 4, pp. 1801–1810, 2014.

[27] S. E. Lee, E. C. B. Olsen, and W. W. Wierwille, “A Comprehensive Examination of Naturalistic Lane-Changes,” 2004.
[28] T. Lee, B. Kim, K. Yi, and C. Jeong, “Development of lane change driver model for closed-loop simulation of the active safety system,” *IEEE Conf. Intell. Transp. Syst. Proceedings, ITSC*, pp. 56–61, 2011.
[29] T. Toledo and D. Zohar, “Modeling Duration of Lane Changes,” *Transp. Res. Rec. J. Transp. Res. Board*, vol. 1999, pp. 71–78, 2007.
[30] C. Michaels, D. Kelley, R. Sumner, S. Chriss, and DCK & Suz, “DSRC Implementation Guide A guide to users of SAE J2735 message sets over DSRC,” *Communication*, p. 210, 2010.
[31] G. P. Stein, O. Mano, and A. Shashua, “Vision-based ACC with a single camera: Bounds on range and range rate accuracy,” in *IEEE Intelligent Vehicles Symposium, Proceedings*, 2003, pp. 120–125.
[32] Q. Luo, J. Auld, and V. Sokolov, “Addressing some issues of map-matching for large-scale, high-frequency GPS data sets Qi,” in *Transportation Research Board 95th Annual Meeting*, 2015.
[33] S. Kotz and S. Nadarajah, *Extreme Value Distributions*. PUBLISHED BY IMPERIAL COLLEGE PRESS AND DISTRIBUTED BY WORLD SCIENTIFIC PUBLISHING CO., 2000.
[34] A. H. Haddad, *Applied optimal estimation*, vol. 64, no. 4. 1976.
[35] C. Rose, “Lane Level Localization with Camera and Inertial Measurement Unit using an Extended Kalman Filter,” 2010.
[36] Transportation Research Board, “75 Years of the Fundamental Diagram for Traffic Flow Theory. Greenshields Symposium,” *Transp. Res. Circ.*, vol. E-C149, no. June, pp. 45–62, 2011.
[37] C. M. Bishop, *Pattern Recognition and Machine Learning*. 2006.
[38] S. Sun, C. Zhang, and Y. Zhang, “Traffic flow forecasting using a spatio-temporal bayesian network predictor,” in *Artificial Neural Networks: Formal Models and Their Applications--ICANN 2005*, 2005, pp. 273–278.
[39] *Highway capacity manual 2010*. 2010.
[40] H. H. Yang and H. Peng, “Development of an errorable car-following driver model,” *Veh. Syst. Dyn.*, vol. 48, no. 6, pp. 751–773, 2010.
[41] D. Branston, “Models of Single Lane Time Headway Distributions,” *Transp. Sci.*, vol. 10, no. February 2016, pp. 125–148, 1976.
[42] J. Fox and S. Weisberg, “Robust Regression,” *Behav. Res. Methods*, vol. 1, no. January, pp. 1–8, 2002.
[43] V. Ramanujam, “Lane Changing Models for Arterial Traffic,” *Environ. Eng.*, no. 2005, 2007.
[44] D. Zhao, “Accelerated Evaluation of Automated Vehicles,” 2016.
[45] “Mcity Test Facility - Mcity.” [Online]. Available: https://mcity.umich.edu/our-work/mcity-test-facility/. [Accessed: 03-Jul-2018].